Methane emissions from oil and gas production on the North Slope of Alaska

Cody Floerchinger[1], Kathryn McKain[2,6], Timothy Bonin[3,6], Jeff Peischl[3,6], Sébastien C. Biraud[4], Charles Miller[5], Thomas B. Ryerson[3], Steven C. Wofsy[1], Colm Sweeney[2]

1. Department of Earth and Planetary Sciences, Harvard University, Cambridge, MA

2. Earth System Research Laboratory, Global Monitoring Division (GMD), National Oceanic and Atmospheric Administration, Boulder, CO, USA

3. Earth System Research Laboratory, Chemical Science Division (CSD), National Oceanic and Atmospheric Administration, Boulder, CO, USA

4. Climate Sciences Department, Lawrence Berkeley National Laboratory, Berkeley, CA

5. Jet Propulsion Laboratory, California Institute of Technology, Pasadena, CA

6 Cooperative Institute for Research in Environmental Sciences (CIRES), University of Colorado, Boulder, Colorado, USA

Correspondence: codyfloerchinger@g.harvard.edu
(907)-529-1811
20 Oxford St, Cambridge, MA, 02138

Abstract

Recent warming of the Arctic has motivated assessments of methane (CH_4) release from the North Slope Region of Alaska (NSRA). This study examines the contributions of thermogenic emissions from the Prudhoe Bay Oil Field (PBOF) to the elevated concentrations of atmospheric CH_4 observed across the NSRA. We report high precision atmospheric measurements of CH_4 and ethane (C_2H_6) within and downwind of the PBOF. Biogenic CH_4 emissions, due to methanogenic processes within the Arctic tundra, are not co-emitted with C_2H_6. We show that the thermogenic gas emanating from oil and gas extraction point sources contains on average 1 mole of C_2H_6 for

every 16 moles of CH_4. We use a mass balance approach to estimate total emissions of thermogenic CH_4 from two days in the summer of 2016 and find 2 - 5 times greater emissions than the sum of all sources in the PBOF reported to the EPA Greenhouse Gas Reporting Program in 2016. Although higher than reported, these emissions are much smaller than estimates of CH_4 emissions from other oil and natural gas production areas in the US, and they make a very small contribution to total CH_4 emissions from the North Slope.

Keywords: Prudhoe Bay, Fugitive Methane Emissions, Thermogenic Methane, Arctic Methane Emissions, Oil and Gas Methane Emissions

Introduction

Methane (CH_4) is the second most potent anthropogenic greenhouse gas. Methane emissions have been a particular concern in the Arctic, where warming temperatures could cause massive amounts of organic carbon trapped in the active layer of the permafrost (Hugelius et al., 2014) to be decomposed under anoxic conditions to produce large amounts of atmospheric CH_4.

Elevated atmospheric concentrations of CH_4 have traditionally been observed throughout the North Slope Region of Alaska (NSRA), located on Alaska's northern coast and bounded at the southern edge by the foothills of the Brooks Range (Figure 1). The dominant source of these CH_4 enhancements is generally understood to be biological metabolism of soil organic matter stored in the active layer of the permafrost(McGuire et al., 2012). A number of recent studies have sought to quantify the flux, seasonality, and environmental factors that drive these emissions within the NSRA(Chang et al., 2014; Miller et al., 2016; Colm Sweeney et al., 2016; Zona et al., 2016), but there has been a persistent concern that a significant fraction of the observed CH_4 enhancement could originate from petroleum production at the nearby Prudhoe Bay Oil Field (PBOF).

Prudhoe Bay Oil Field is situated on top of a deep sandstone formation near the town of Deadhorse, Alaska in an area roughly 80x50 km^2 in size. Thermogenic hydrocarbon gases and crude oil are formed in the sandstone at a depth of around 2,500 meters below the surface by thermal alteration of organic matter at high temperatures and pressures (*AOGCC* 2018). PBOF is nominally an oil producing field, but large amounts of natural gas (3.1 trillion cubic feet per year ($TCFy^{-1}$) are co-produced and ultimately reinjected into the formation to ensure the oil remains recoverable *(AOGCC*, 2018). Until now, the total flux of fugitive and process CH_4 emissions from PBOF has never been quantified by top-down methods due to the complexity associated with trying to measure a concentrated CH_4 source in the midst the diffuse CH_4 emissions from the Arctic tundra.

The present study quantified thermogenic CH_4 emissions from PBOF with a series of aircraft flights which surveyed concentrations of atmospheric CH_4 and C_2H_6 to quantify the relative enhancement of thermogenic CH_4, which is co-emitted with C_2H_6, versus biogenic emissions, which are not. We determined the mean CH_4: C_2H_6 ratio from PBOF facilities, and then used a mass balance approach to determine the total flux of C_2H_6 coming from PBOF. From the mean CH_4: C_2H_6 ratio and the C_2H_6 flux it is possible to determine the CH4 emissions coming from thermogenic sources in the PBOF. Subsequent measurements made during the campaign over the widespread NSRA, outside of PBOF, can be used to qualitatively evaluate the contributions of thermogenic gas from deep geologic reservoirs to widespread CH_4 enhancements observed over the Alaskan Arctic in the height of the growing season.

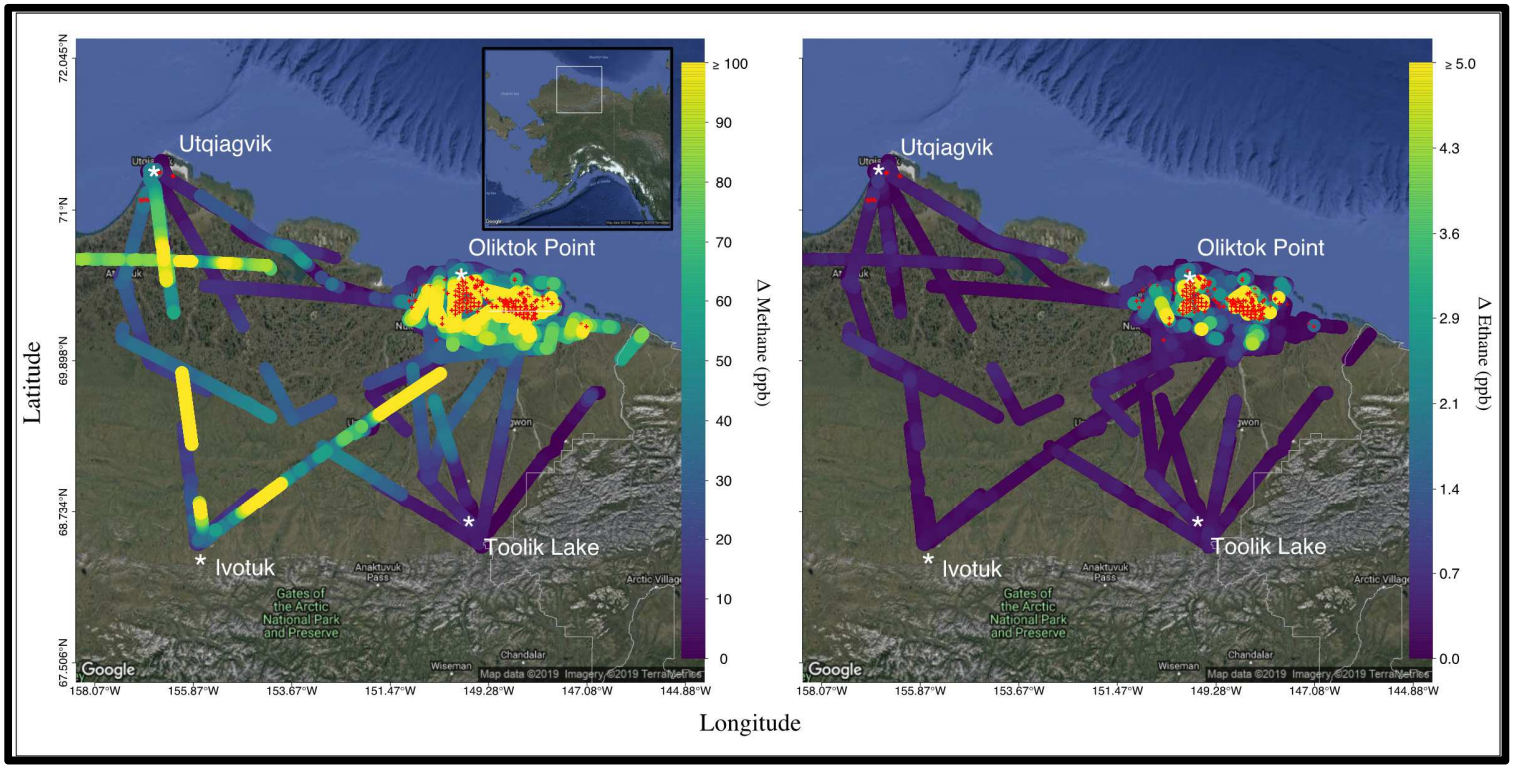

Figure 1 Methane and C_2H_6 enhancements (ΔCH_4 & ΔC_2H_6) measured within the planetary boundary layer over background concentrations measured in the free troposphere with aircraft vertical profiles on all campaign flights over the NSRA. Red dots show the location of operational wells in the PBOF. The inset map shows the location of the NSRA study domain within the state of Alaska.

Methods

Measurement Description

Measurements were made on a National Oceanographic and Atmospheric Administration (NOAA) Twin Otter aircraft based in Deadhorse, Alaska from July 24th to August 21st of 2016. The aircraft was instrumented with a Cavity Ringdown Spectrometer measuring CO_2, CO, CH_4, and H_2O at ~0.3Hz resolution with precision of ~ 50, 4, 0.4, and $3x10^4$ ppb ($\frac{nmol}{mol\ air}$)in 5 seconds, respectively. (Picarro, Model G2401)(Crosson, 2008). Ethane was measured at 1Hz using an infrared laser spectrometer manufactured by Aerodyne Research (Yacovitch et al., 2014), modified for flight as described below. The dry mole fractions of CH_4, CO_2, and CO were computed from

77 the Picarro H_2O data using an analyzer-specific empirical correction derived from laboratory-
78 based tests (Chen et al., 2013; Rella et al., 2013). In-situ measurements of CH_4, CO_2, CO, and
79 C_2H_6 were calibrated using in-flight inlet overblow injections of calibrated tank air traceable to
80 World Meteorological Organization (WMO) and NOAA scales (CO_2-X2007; CH_4–X2004A; CO–
81 X2014A, www.esrl.noaa.gov/gmd/ccl/).

82 To provide an independent check on the compatibility of in-situ measurements and the
83 larger array of ground-based trace gas measurements in the region, flask samples were also
84 collected throughout each flight (roughly 24 per flight) and analyzed at the NOAA Earth System
85 Research Laboratory in Boulder, Colorado (Sweeney et al., 2015). Along with CH_4, CO_2, CO, and
86 C_2H_6, flask samples were analyzed for several additional hydrocarbons, halocarbons, fluorinated
87 gases, and isotopes of CH_4. Wind speed and direction were measured at 10Hz using an Aventech
88 AIMMS-30 differential pressure wind probe. Additional measurements included GPS position and
89 ambient pressure (from the Picarro located in the unpressurized airplane cabin), temperature, and
90 relative humidity (Vaisala HMP60).

91 Ethane measurements were made with an Aerodyne Research Inc. Mini Tunable Infrared
92 Differential Laser Absorption Spectrometer (ARI-TILDAS) based on direct absorption
93 spectroscopy, in which a mid-infrared light source is passed through a multi-pass Herriot cell with
94 an effective path length of 76m (McManus et al., 2008). Recent upgrades in interband cascade
95 laser technology enabled the ARI-TILDAS to interrogate the rotational-vibrational infrared
96 absorption of an C_2H_6 molecule at the 2997 cm^{-1} q-branch. Spectra were fit based on
97 experimentally determined absorption parameters (Harrison et al., 2010; Yacovitch et al., 2014).

98 Prior to field deployment, the C_2H_6 instrument precision was characterized over a typical
99 2-hour flight out of Boulder, CO which climbed from 1600 to 8000 meters above sea level by

measuring a single tank of dry gas and overflowing excess sample across the inlet to provide ambient pressure to the sample line. After drift correcting based on zero gas injections every 10 minutes, the 1s root mean squared deviation (RMS) from the calibrated tank value was 65 pptv. After shipment to Alaska and realigning the instrument optics, the inflight 1s RMS was < 40 pptv, and with precision better than 10 pptv when the data were averaged over 17 s intervals (Supplemental section 1.1). Observed concentration changes in C_2H_6 were small compared to its background concentration (~0.5 ppb), and the high measurement precision of C_2H_6 was essential to distinguish and accurately measure emission-related signals over the background. The high precision and measurement frequency (1 Hz) that can be obtained from the C_2H_6 spectrometer makes it a more accurate tracer for thermogenic CH_4 emissions when compared to traditional methods such as isotopic CH_4 measurements(Sayres et al., 2017).

Flight Patterns

Over the course of the campaign, 14 research flights were flown for a total of >90 hours of airborne data. All fights took off from Deadhorse, AK. Ten flights were designed to capture the large-scale CH_4 and C_2H_6 variability over NSRA and provide continuity with other multi-year aircraft datasets collected over the Alaskan tundra (Chang et al., 2014; Commane et al., 2017; Hartery et al., 2018; Parazoo et al., 2016). NSRA flights covered a region bounded by Toolik Lake, Ivotuk, Utqiaġvik (formerly Barrow) and Deadhorse (Figure 1). These flights typically required landing in Utqiaġvik to refuel before returning to Deadhorse.

We flew 4 flights designed to quantify CH_4 emissions from the PBOF using a mass balance analysis. These flights were flown in a box pattern with the headings of individual legs determined by the mean wind direction. At least one leg of each flight was flown at a constant altitude

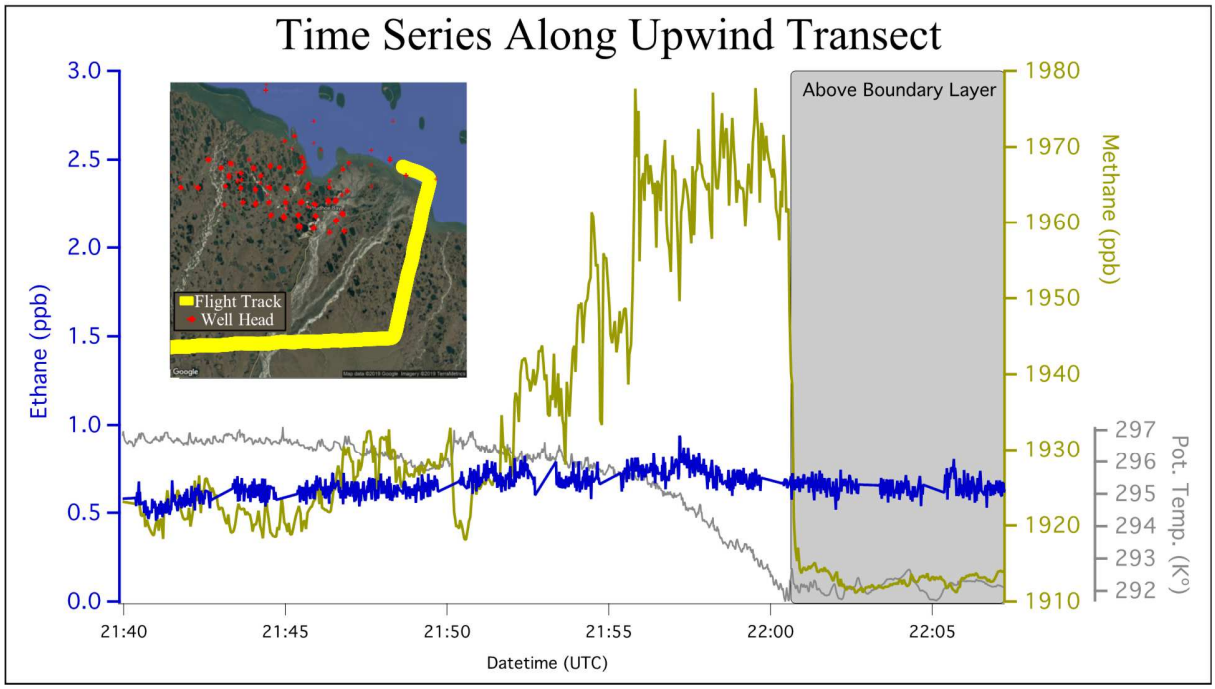

Figure 2 Time series of CH_4, C_2H_6, and potential temperature measured on the transect upwind of the PBOF on 2016-08-06. A strong biogenic CH_4 enhancement is observed below the boundary layer while C_2H_6 is constant above and below the boundary layer. The boundary layer can be identified using the potential temperature signal shown in the lower portion of the right axis. The direction of flight on this transect was south and then westbound.

perpendicular to the mean wind direction, downwind of the PBOF and far enough from the majority of point sources to allow enhancements to mix homogenously throughout the PBL (Karion et al., 2013). Of the 4 mass balance flights, 2 flights had steady enough winds to allow for predictable transport across the study domain and stable enough horizontal winds within the planetary boundary layer (PBL) to allow for strong vertical mixing of emissions from the ground upwards required for the mass balance method (Cambaliza et al., 2014).

An upwind leg was flown perpendicular to the prevailing winds each day to determine the background mole fractions of C_2H_6 and CH_4 and to confirm that there were no detectable sources of C_2H_6 upwind of the PBOF. The mean background value measured on the upwind side of the mass balance domain was subtracted from the downwind transects in order to compute the

enhancement used in the mass balance calcualation. The background transect was defined based on the observation of a consistent upwind C_2H_6 mole fraction as shown in Figure 2. The inset in Figure 2 shows an example of how the background flight tracks were positioned well upwind of potential sources. By flying a vertical profile through the PBL on the upwind side of PBOF, we were able to confirm that there was no gradient in C_2H_6 above and below the PBL, which further supports the inference that there were no significant sources of C_2H_6 upwind of PBOF. Each flight included a vertical profile up to the free troposphere to determine the height of the PBL, the homogeneity of CH_4 and C_2H_6 within the PBL, and the gradients in CH_4 and C_2H_6 between the PBL and the free troposphere.

Two flights within the PBOF circled several individual facilities at a distance of ~0.5 km, in order to measure the molar ratio of CH_4:C_2H_6 in the natural gas being emitted from these facilities. A total of 71 plumes were measured to derive an average CH_4:C_2H_6 molar ratio. These plumes were readily identified from the data and the ratio of mole fraction enhancements in each of these plumes was determined by fitting a scatterplot of C_2H_6 versus CH_4 for each plume using an ordinary least squares regression (errors are attributable mainly to the C_2H_6 data). Because the temporal profile of these plumes was short (approximately 5-10 seconds) and the enhancements were very high due to the close proximity of the aircraft to the facility, it was assumed that the background was invariant for these short plumes. The average r^2 value of the fitted plumes was 0.74. The median CH_4:C_2H_6 enhancement ratio (EMER) $\left(\frac{moles\ CH_4}{moles\ C_2H_6}\right)$ and its 95% confidence interval were determined for the PBOF by iteratively subsampling the distribution of slopes calculated for each plume. Section 2.1 of the supplement shows the measured and bootstrapped distributions of the EMER and further describes this methodology.

Lidar Measurements of Planetary Boundary Layer Height

Data from a pulsed Doppler Lidar (Halo Streamline) operated at the Atmospheric Radiation Measurement mobile facility at Oliktok Point, Alaska (https://www.arm.gov/capabilities/observatories/nsa) was used to determine the boundary layer winds before the aircraft took off, and to define the coastal boundary layer height in the PBOF. The Lidar measures line-of-sight velocity and backscatter at ≈ 0.6 Hz with a range resolution of 18m. A detailed description of the system design and operating principles of the Doppler Lidar can be found in Pearson, Davies, & Collier 2009 (Pearson et al., 2009). Every 10 min, the Lidar took 35s to perform an eight-point plan-position-indicator scan at 70 degrees in elevation above the horizon to measure the horizontal wind speeds. Otherwise, the Lidar pointed vertically to observe the vertical wind speed and aerosol backscatter. These vertically pointing measurements were processed in 10-min bins to compute the vertical velocity variance (σ_w^2) and mean backscatter profiles.

Vertical profiles of these measured quantities (i.e., mean wind, σ_w^2, aerosol backscatter) were combined to determine the PBL height at Oliktok Point using fuzzy logic (Bonin et al., 2017). Since the turbulence was generally weak ($\sigma_w^2 < 0.2$ m^2 s^{-2}), likely due to the proximity of the cold ocean surface which acts to stabilize the PBL, the backscatter profiles were the dominate factor in determining the PBL height. Large gradients in the backscatter, typically located at the top of the PBL between the aerosol rich air in the PBL and clean air in the free troposphere, were detected by running a Haar wavelet (Haar, 1910) over the backscatter profile to deduce the PBL height. Boundary layer heights at Oliktok Point during the two days used in the mass balance analysis of PBOF are shown in supplemental section 3.1.

Mass Balance Analysis

177 Analysis of available operational meteorological models with domains covering the PBOF
178 region showed that the PBL height was significantly over estimated, failing to reproduce the inland
179 intrusion of the cold air from the marine boundary layer. Given the lack of reliable meteorological
180 models, our estimate of total emissions from the PBOF employed the simplifying assumptions of
181 a mass balance (Cambaliza et al., 2014; Karion et al., 2013) combined with our direct
182 measurements of winds, PBL height and C_2H_6 enhancements. Estimated emissions of C_2H_6 were
183 combined with the EMER to derive the flux of thermogenic CH_4 from the PBOF.

$$Flux_{C_2H_6} = \int_{-bck}^{bck} X_{C_2H_6} \left(\int_{Z_{surface}}^{Z_{PBL(x)}} n_{air} * WS * dz \right) \cos(\theta) dx$$

Equation 1 Where (-bck and bck) represent the background concentraitions at the "edges" of each downwind plume, X_{C2H6} represents the C_2H_6 enhancement above the background concentration (determined from the upwind profile), n_{air} represents the density of air within the PBL. WS represents the mean wind speed across the domain, and cos(ø) represents a correction for the non-orthogonality of the flight track with respect to the prevailing wind direction (ø being the amount of degrees that the flight track is deviating from the normal wind direction).

184 Total emissions of C_2H_6 were estimated by integrating the horizonal mass flux of air (n_{air}
185 * WS, $mol_{air}/(m^2s)$) from ground level ($Z_{surface}$) to the top of the PBL (Z_{PBL}) along the downwind
186 transect perpendicular to the wind, then multiplying by the C_2H_6 enhancement (X_{C2H6}) and
187 integrating along the length of the downwind track. For the mass balance experiments the
188 downwind C_2H_6 enhancement was computed by subtracting the mean upwind C_2H_6 mole fraction
189 measured in the upwind transects from the downwind measurement. Wind measurements from the
190 aircraft indicated that there were only minor gradients in winds throughout the PBL. A distribution
191 of the measured wind speed is used in the final calculation to estimate the contribution of
192 variability in winds to the total uncertainty. We assumed the enhancement of C_2H_6 was constant
193 from the surface ($Z_{surface}$) to the top (Z_{PBL}) of the PBL based on vertical profile measurements

194 (Supplement, Section 3.2) and because the downwind track was far enough away from the major
195 point source emissions to allow for complete vertical mixing of point source plumes through the
196 PBL(Karion et al., 2013)

197 A piecewise integral of the molar volume of air (n_{air}, mol_{air}/m^3) from the surface to the
198 top of the PBL at each meter along the downwind transect was performed to correct for changes
199 in both topography and the height of the PBL along the flight track. The ground elevation
200 coordinate was calculated using the USGS Elevation Point Query Service (Hollister, 2017). The
201 PBL height was determined from vertical profile measurements as the altitude where there was a
202 significant gradient in potential temperature, water vapor and CH_4 (Figure S3.2A). The pulsed
203 doppler Lidar was also used to measure the height of the PBL at the northern most part of the
204 transects where the colder marine air mixed with the warmer inland air and suppressed the height
205 of the height of the mixed layer. The height of the PBL along the flight track was estimated by
206 interpolating between the PBL heights measured by the coastal pulsed Doppler Lidar and the
207 aircraft profile nearest to the southern side of the PBOF domain. Our assumption of a linear
208 gradient in the PBL height is supported by a steady decrease in potential temperature as the aircraft
209 headed toward the coast during the downwind transects indicating that the change in boundary
210 layer height was not abrupt as caused by a frontal system. A discussion of our method for
211 approximating the effect of the marine layer on the PBL height and a conservative estimate of
212 potential errors associated with this model is presented in section 3.3 of the supplemental
213 information.

214 We used the HYSPLIT model (Stein et al., 2015) run forward in off-line STILT (Lin et al.,
215 2003) mode and driven by metrological products from the Global Forecast System (GFS), to verify
216 that winds were steady across the PBOF domain previous to the time at which downwind plumes

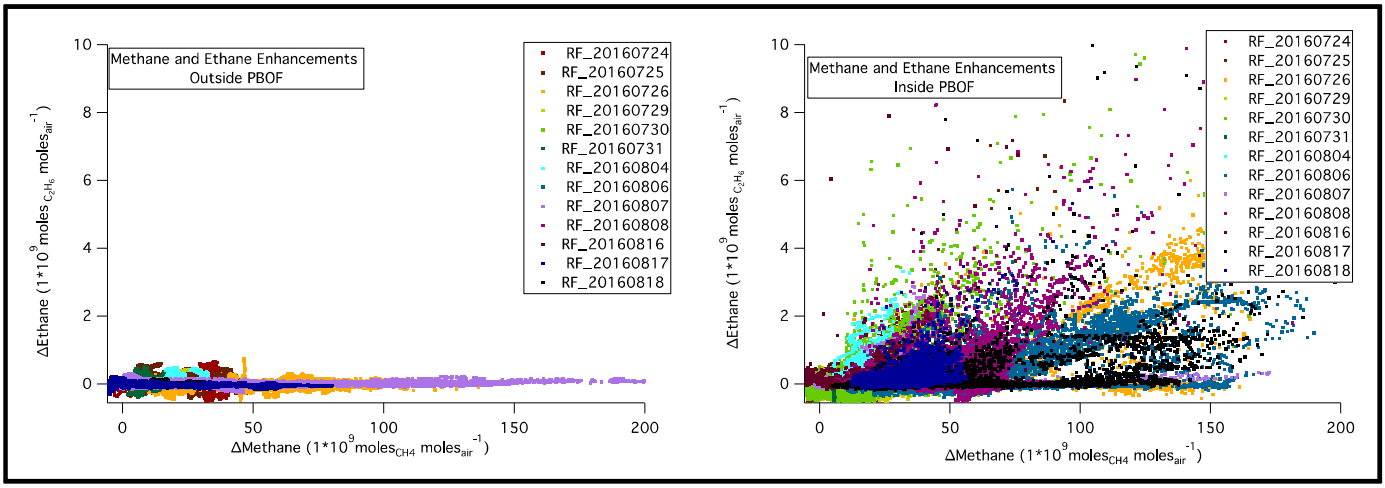

Figure 3 Shows a tracer-tracer plot of all data within the Planetary Boundary Layer measured inside and outside of PBOF.

were sampled by the aircraft. The HYPLIT model was also used to confirm that downwind enhancements of thermogenic CH_4 measured by the aircraft were consistent with the spatial distribution of point sources reported in the Greenhouse Gas Reporting Program (GHGRP). The details of the HYSPLIT analysis are shown in section 4 of the supplement. Due to inaccuracies in the GFS PBL height, further analysis of this data using either forward or inverse modelling approaches was not possible.

Results

Regional scale distribution of CH_4 and C_2H_6

Figure 1 shows the PBL enhancements above background of CH_4 and C_2H_6 for all 14 flights within NSRA. Enhancements above background were calculated by subtracting free tropospheric mole fractions (nominally 0.6 ppb and 1913 ppb for C_2H_6 and CH_4) measured during aircraft vertical profiles on each day. Methane enhancements were very widespread outside of the PBOF, reaching maximum values > 150 ppb. In sharp contrast, enhancements of C_2H_6 were limited almost exclusively to the PBOF and areas affected by PBOF outflow.

Figure 3 shows CH_4 and C_2H_6 enhancements within the PBL (enhancement above free tropospheric values measured during vertical profiles throughout each flight) for flight segments outside and inside of the PBOF. Figure 3 illustrates both the lack of C_2H_6 enhancements and the prevalence of large CH_4 enhancements outside of PBOF . Section 5 of the supplemental information shows the timeseries from inside and outside of PBOF and shows the different spatio-temporal characteristics of mole fraction enhancements that result from point source emissions found in the PBOF versus the regional-scale biogenic emissions found in the NSRA outside of the PBOF region.

Meteorological conditions

The spatial distribution of the particles in the HYSPLIT model output indicates that winds were coming from approximately 120^0 and 325^0 on 06 August and 08 August, 2016 respectively. The modeled wind directions agree with the wind directions measured by the aircraft for each transect (Table S4.3A). Measured 1Hz wind speeds from the aircraft were $5.4 \pm 1.2 \frac{m}{s}$ and $6.1 \pm 1.5 \frac{m}{s}$ on 06 August and 08 August, 2016. We estimate that the transport time of an airmass across the PBOF (approximately 80km) was roughly 4 hours during our study days. Analysis of mean particle trajectories from HYSPLIT and the spatial distribution of individual particles suggests that the flow was steady and consistent across the domain prior to and during the flights. There was evidence of horizontal wind shear that could have potentially caused PBOF emissions to be advected out the side of our mass balance domain.

Further analysis of the vertical gradient in backscatter and vertical wind observed by the pulsed Doppler Lidar, as well as the aircraft vertical profiles, shows that mixing between the PBL and free troposphere was negligible. The pulsed Doppler Lidar shows that small vertical motions associated with the weak updrafts generally at the mixed layer boundary were not able to penetrate

into the free troposphere thus validating the assumption in the mass balance calculation that there is minimal detrainment (leakage) into the free troposphere from the PBL.

Measured PBL height values range from approximately 90 magl at the coastal Lidar to 525 magl at the inland aircraft vertical profile. The differences in the measured PBL height between the Lidar site and the aircraft profiles, determined based on mole fraction and meteorological measurements, were consistent with the expected spatial gradient in PBL height between the marine PBL near the coast and the well-developed PBL inland.

Mass Balance

The EMER determined from two flights dedicated to surveying the composition of point sources in the PBOF was very stable at 16.6 $\pm$ 0.74 (mol CH_4 / mol C_2H_6; 95% confidence interval). Five transects were flown downwind of the PBOF on 06 August 2016 and one transect was flown on 08 August 2016. Flux estimates from each of the 6 realizations of the mass balance experiment are shown in Figure 3. The total flux was consistent between the two days, indicating that emission sources were stable over those two days.

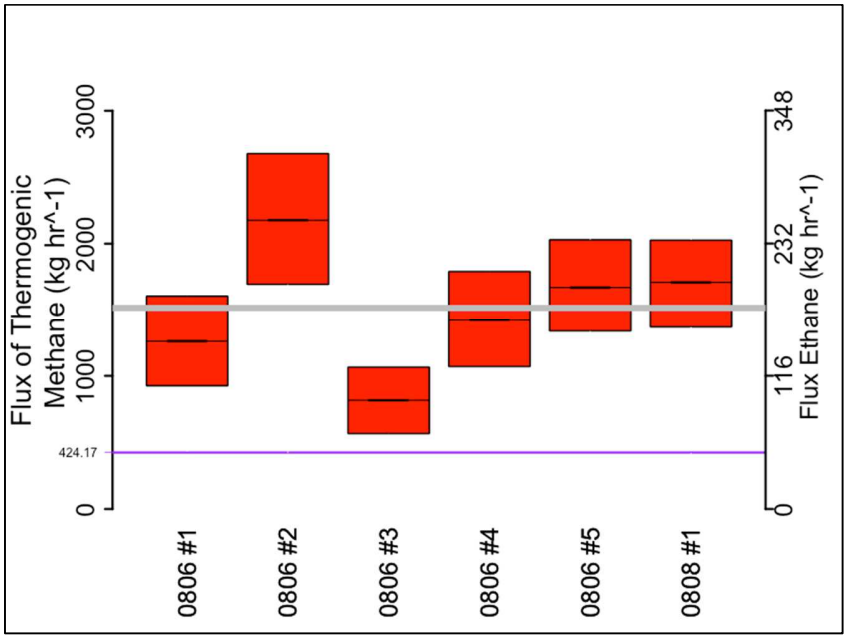

Figure 4 Flux estimates from six realizations of the mass balance experiment conducted on two different days. The height of the box represents one standard deviation in the estimated flux distribution in order to show the spread of the error associated with each estimate. The gray line represents the median flux calculated from the six realizations. The purple line marks the total CH_4 emissions from the PBOF in the 2016 GHGRP. The transect locations are shown on a map in figure S4.1A.

From the ensemble of transects collected, an estimated flux of 1500 [1151, 1888] kg/hr (95% Confidence Interval) of thermogenic CH_4 was emitted by the PBOF during the two days with measurements in the summer of 2016. Our confidence intervals for each transect include an additional uncertainty of 20% for the PBL height to capture the difference in the PBL height as measured by the Lidar at Oliktok Point and by the aircraft vertical profiles inland. Total uncertainty in the flux estimate was estimated for each downwind transect by iteratively subsampling probability density functions of aircraft meteorological data (winds speed and direction), boundary layer height (obtained by interpolating the height measured at the inland profile and at the Oliktok Point Lidar and adding an additional 20% error), and EMER (from the bootstrapped distribution of the survey plumes), then iteratively computing the mass balance flux by equation 1 for each flight transect. The overall error of the total flux (1500 [1151, 1888] kg/hr) is contained with the 95% confidence interval of the convolution of flux distributions from each transect. The relative magnitude of our error estimate is comparable to other studies using similar top-down methodology(Cambaliza et al., 2014; Heimburger et al., 2017) and to that obtained by a individually summing each source of proportional error in quadrature.

Discussion

North Slope Region

Our large-scale measurements of CH_4 over the NSRA, specifically those parts to the west and south of PBOF (Fig 1), are consistent with observations made near Utqiaġvik and throughout the region that show large enhancements of CH_4 coming from the tundra area (Chang et al., 2014;

293 Miller et al., 2016; Sweeney et al., 2016). Furthermore, these large enhancements do not appear to
294 originate from point sources within the NSRA, based on their relatively small spatial variability
295 (tens of kilometers) when compared to the point source enhancements in PBOF (tens of meters).
296 The emissions outside of the PBOF are not significantly thermogenic, based on the lack of
297 observed C_2H_6 enhancements (Fig 3), supporting other studies(Chang et al., 2014; Miller et al.,
298 2016; Sweeney et al., 2016) which suggested that most of the CH_4 enhancement over the North
299 Slope was of biogenic origin. We cannot rule out geogenic contributions from diffuse seeps of
300 shallow origin, e.g. from coalbed CH_4, where the associated C_2H_6 signal might be much smaller
301 than for the deep gas in the PBOF and other thermogenic reservoirs. Our results demonstrate that
302 emission of thermogenic CH_4 from deep reservoirs within PBOF is emitting at rates too low to be
303 considered a major factor in the total CH_4 enhancement observed throughout the North Slope
304 Region of Alaska.

305 We further contextualize our estimate of CH_4 emissions from PBOF by comparing it to an
306 estimate of total CH_4 emissions from the NSRA from the literature. Based on the estimated CH_4
307 flux from the North Slope and the total area from their chosen land mask, Chang et. al. 2014
308 calculates total CH_4 emissions in NSRA during the peak of the growing season (May-September)
309 to be approximately 52 +/- 15 * 10^3 kg * hr^{-1}, suggesting that thermogenic CH_4 emissions from
310 PBOF are responsible for approximately 2.8% [1.68% - 4.85%] of the total CH_4 emissions from
311 the NSRA during the growing season (Chang et al., 2014) Biogenic CH_4 emission from the tundra
312 displays a strong seasonal dependence with near zero fluxes throughout the winter (Zona et al.,
313 2016), whereas we assume that PBOF thermogenic emissions do not vary with season, suggesting
314 that the fraction of total annual CH_4 emissions from PBOF would be larger than 3% . Nevertheless,

315 the total CH_4 flux from PBOF is a small compared to the total CH_4 emissions throughout the
316 NSRA.

317 **Prudhoe Bay Oil Field**

318 PBOF is the largest oil field in Alaska, producing approximately 97% of the oil from the
319 state. Oil from PBOF is carried 800 miles via the Trans-Alaska Pipeline System from Deadhorse
320 to Valdez, AK where it is either refined or tankered and exported to market.(*AOGCC*, 2018) With
321 no way to transport the co-produced natural gas, it is first dehydrated and then either reinjected to
322 facilitate future recovery of liquid crude, flared, or used as an onsite fuel source (*British Petroleum*
323 *Fact Sheet: Gathering Centers , Flow Stations*, 2011). Despite a large drop in oil production since
324 the PBOF opened in 1977, the amount of co-produced natural gas has remained relatively constant
325 throughout the lifetime of the field(*AOGCC*, 2018) (Figure S6.1A). Total CH_4 emissions reported

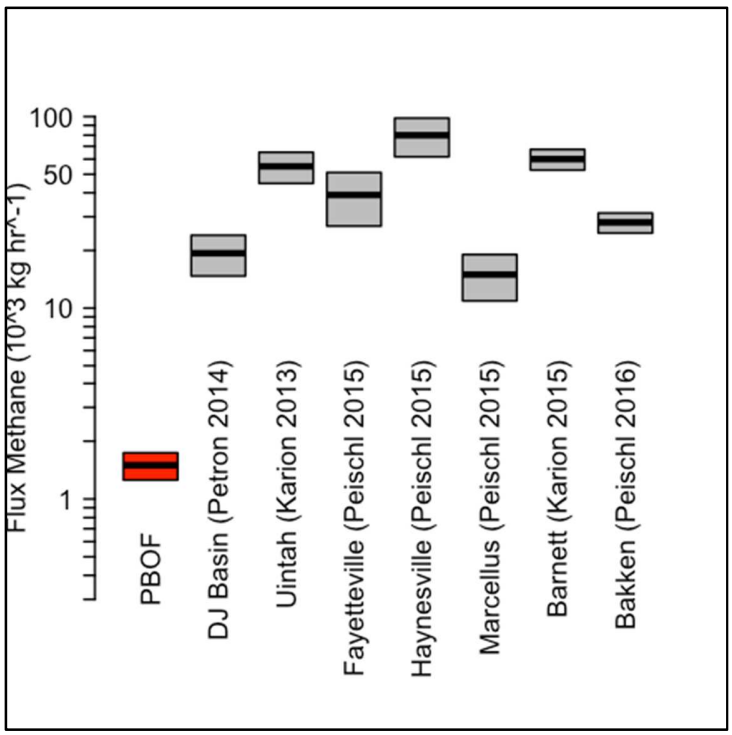

Figure 5 Methane emission rates from oil and gas producing regions in the United States estimated using top-down methods.

to the EPA GHGRP(EPA, 2018) for 2016 from the PBOF are ~420 kg/hr(EPA, 2018). This rate is 23% lower than emissions reported to the GHGRP in 2015, partly due to 35% fewer sites in PBOF reporting to the GHGRP in 2016 and partly because the largest emitting sites reported significantly less emissions than in previous years. Though the GHGRP is not designed to be a comprehensive bottom up emission inventory, it is a helpful metric to compare to our results and the best available benchmark for PBOF emissions during our study. We find that CH_4 emissions for the PBOF from the 2016 GHGRP were lower than the total emissions measured by our mass balance analysis by a factor of 2-5. Our results are consistent with previous studies that have shown CH_4 emissions by production facilities are underestimated in reporting to the GHGRP and other emission inventories. (Alvarez et al., 2018; A. R. Brandt et al., 2014)

Because recent oil and gas production in the contiguous United States has shifted to using unconventional methods (hydraulic fracturing of shale formations) or a mix of both conventional and unconventional methods, and basins employing conventional methodology (such as PBOF) have not been as extensively measured using top-down methodologies, we contextualize our results against recent CH_4 emission estimates from unconventional oil and gas developments. (A R Brandt et al., 2014; Karion et al., 2015, 2013; Peischl et al., 2016; Pétron et al., 2014) Though gas production varies regionally, our estimates of the absolute CH_4 emissions from PBOF are significantly lower than absolute emission estimates from other oil and gas production regions when studied using similar mass balance methodologies (Figure 5).

Survey flights sampling plumes from major point sources in the PBOF showed highly variable ratios of C_2H_6 to CO_2 enhancements, even though C_2H_6 to CH_4 ratios were very consistent (Supplement, Section 5.1), suggesting that thermogenic CH_4 originates from both onsite leakage and incomplete combustion processes. Possible combustion sources include onsite flaring, which

was often observed from the aircraft, and natural gas fueled compressors used for local gathering or reinjection, both of which are listed in the GHGRP inventory and the Alaska Oil and Gas Conservation Commission (AOGCC) database .(EPA, 2018; *AOGCC)* 2018)

In 2016, 3.1 trillion cubic feet per year ($TCFy^{-1}$) of natural gas were withdrawn from 2,071 gas producing oil wells in Alaska, the vast majority of which was from the PBOF(*AOGCC*, 2018) (Fig S61.A). Reinjecting produced natural gas in the PBOF requires much simpler system infrastructure than production for sale, and the PBOF lacks the extensive gathering, processing, and transmission facilities that are present in most oil and gas production regions in the contiguous U.S. For comparison, the Bakken oil field in North Dakota has 13,253 gas producing oil wells that withdraw 0.6 $TCFy^{-1}$ of natural gas, 1/5 as much as the PBOF. Due to improved infrastructure in recent years, 0.53 $TCFy^{-1}$ of gas from North Dakota now goes to market, only 0.07 $TCFy^{-1}$ is vented or flared, and none is reinjected, consistent with most oil producing regions in the contiguous U.S. (EIA, 2018). Regions that are predominantly natural gas producing, such as the Marcellus shale region in Pennsylvania, withdraw larger volumes of natural gas (5.3 $TCFy^{-1}$) from natural gas specific wells and all of the gas is processed and sent to market as opposed to being reinjected. We speculate that the low CH_4 emission rates calculated for PBOF compared to other oil and gas producing regions (Fig. 4) are due to the simple produced gas handling infrastructure and the immediate reinjection of produced gas back into the geologic formation in PBOF. Simply put, the gas produced in PBOF spends less time above ground where potential leaks to the atmosphere may occur, whereas in more complex fields with gathering and sales infrastructure, produced natural gas flows past many more potential leak points before making it to the end user.

Our analysis shows a snapshot in time (2 days) and provides no information on how consistent PBOF emissions have been over time. Oil production from the PBOF has been declining

steadily since its peak production of over 2 million barrels per day in the early 1990's to its current, all-time low, production of ~450,000 barrels per day in 2016 (Supplement, Section 6). (*AOGCC*, 2018; EIA, 2018) Reinjection of the produced natural gas and a decline in recoverable oil has led to an increase in the gas to oil ratio in the field resulting in a relatively stable natural gas production rate of ~3 $TCFy^{-1}$ since the beginning of 1995 (Figure S6.1A). If CH_4 emissions scale with production throughput, as suggested by other studies (Marchese et al., 2015), then it is likely that fugitive emissions from this source may also be stable over long time periods. However, some studies have observed emissions that spike during well completions and abnormal operating conditions such as temporary leaks or unexpected releases, which must be recognized as a caveat when considering the long-term representativeness of the emission rates estimated in our study. (Alvarez et al., 2018)

Summary

High accuracy, high resolution aircraft surveys of C_2H_6 over the NSRA provide new insight into the role of thermogenic CH_4 emissions there. The PBOF is found to be the dominant source of thermogenic CH_4 emissions in the NSRA with flux estimates 2-5 times greater than the sum of the facilities in the region reporting to the EPA GHGRP. However, PBOF emissions are small compared to emissions from other petroleum producing regions in the US. Despite our sensitive indicator for detecting thermogenic emissions, this study found no evidence of significant thermogenic contributions (e.g. co-emissions of C_2H_6) outside of the PBOF in the NSRA.

Acknowledgements:

This work was made possible by funding contributions from NOAA/OCG/AC4 grant #NA14OAR0110140 and NASA Terrestrial Ecology award # NNX17AC61A, "Airborne Seasonal Survey of CO_2 and CH_4 Across ABOVE Domain". We also would like to thank NOAA pilots Lindsey Norman, Frank Centinello and mechanic Robert Miletic for their dedicated service.

References

Agency, U.S.E.P., 2018. Environmental Protection Agency, Greenhouse Gas Reporting Program (GHGRP) [WWW Document]. URL epa.gov/ghgreporting/ (accessed 10.1.17).

Alaska Oil and Gas Conservation Comission (AOGCC), 2018. . Anchorage Alaska.

Alvarez, R.A., Alvarez, R.A., Zavala-araiza, D., Lyon, D.R., Allen, D.T., Barkley, Z.R., Adam, R., Davis, K.J., Herndon, S.C., Jacob, D.J., Karion, A., Kort, E.A., Lamb, B.K., Lauvaux, T., Maasakkers, J.D., Marchese, A.J., Omara, M., Pacala, S.W., 2018. Assessment of methane emissions from the U . S . oil and gas supply chain 7204, 1–9. https://doi.org/10.1126/science.aar7204

Bonin, T.A., Carroll, B.J., Hardesty, R.M., Brewer, W.A., Hajny, K., Salmon, O.E., Shepson, P.B., 2017. Doppler lidar observations of the mixing height in Indianapolis using an automated composite fuzzy logic approach. J. Atmos. Ocean. Technol. JTECH-D-17-0159.1. https://doi.org/10.1175/JTECH-D-17-0159.1

Brandt, A.R., Heath, G.A., Kort, E.A., O'Sullivan, F., Pétron., G., Jordaan, S.M., Tans, P., Wilcox, J., Gopstein, A.M., Arent, D., Wofsy, S., Brown, N.J., Bradley, R., Stucky, G.D., Eardly, D., Harriss, R., 2014. Methane leaks from North American natural gas systems, Supplementary Text and Data File S1. Science (80-.). 342, 733–735.

Brandt, A.R., Heath, G.A., Kort, E.A., O'Sullivan, F., Pétron, G., Jordaan, S.M., Tans, P., Wilcox, J., Gopstein, A.M., Arent, D., Wofsy, S., Brown, N.J., Bradley, R., Stucky, G.D., Eardley, D., Harriss, R., 2014. Methane leaks from North American natural gas systems. Science (80-.). https://doi.org/10.1126/science.1247045

British Petroleum Fact Sheet: Gathering Centers , Flow Stations, 2011.

Cambaliza, M.O.L., Shepson, P.B., Caulton, D.R., Stirm, B., Samarov, D., Gurney, K.R., Turnbull, J., Davis, K.J., Possolo, A., Karion, A., Sweeney, C., Moser, B., Hendricks, A., Lauvaux, T., Mays, K., Whetstone, J., Huang, J., Razlivanov, I., Miles, N.L., Richardson, S.J., 2014. Assessment of uncertainties of an aircraft-based mass balance approach for quantifying urban greenhouse gas emissions. Atmos. Chem. Phys. 14, 9029–9050. https://doi.org/10.5194/acp-14-9029-2014

Chang, R.Y.-W., Miller, C.E., Dinardo, S.J., Karion, A., Sweeney, C., Daube, B.C., Henderson, J.M., Mountain, M.E., Eluszkiewicz, J., Miller, J.B., Bruhwiler, L.M.P., Wofsy, S.C., 2014. Methane emissions from Alaska in 2012 from CARVE airborne observations. Proc. Natl. Acad. Sci. 111, 16694–16699. https://doi.org/10.1073/pnas.1412953111

Chen, H., Karion, A., Rella, C.W., Winderlich, J., Gerbig, C., Filges, A., Newberger, T., Sweeney, C., Tans, P.P., 2013. Accurate measurements of carbon monoxide in humid air using the cavity ring-down spectroscopy (CRDS) technique. Atmos. Meas. Tech. 6, 1031–1040. https://doi.org/10.5194/amt-6-1031-2013

Commane, R., Lindaas, J., Benmergui, J., Luus, K.A., Chang, R.Y.-W., Daube, B.C., Euskirchen, E.S., Henderson, J.M., Karion, A., Miller, J.B., Miller, S.M., Parazoo, N.C., Randerson, J.T., Sweeney, C., Tans, P., Thoning, K., Veraverbeke, S., Miller, C.E., Wofsy, S.C., 2017. Carbon dioxide sources from Alaska driven by increasing early winter respiration from Arctic tundra. Proc. Natl. Acad. Sci. 114, 5361–5366. https://doi.org/10.1073/pnas.1618567114

Crosson, E.R., 2008. A cavity ring-down analyzer for measuring atmospheric levels of methane,

carbon dioxide, and water vapor. Appl. Phys. B Lasers Opt. 92, 403–408. https://doi.org/10.1007/s00340-008-3135-y

EIA, 2018. US Energy Information Administration (EIA) [WWW Document]. www.eia.gov. URL www.eia.gov (accessed 1.1.18).

Haar, A., 1910. Zur theorie der orthogonalen funktionen systeme. Math. Ann. 69, 331–371. https://doi.org/10.1007/BF01456326

Harrison, J.J., Allen, N.D.C., Bernath, P.F., 2010. Infrared absorption cross sections for ethane (C2H6) in the 3 μm region. J. Quant. Spectrosc. Radiat. Transf. 111, 357–363. https://doi.org/10.1016/j.jqsrt.2009.09.010

Hartery, S., Commane, R., Lindaas, J., Sweeney, C., Henderson, J., Mountain, M., Steiner, N., McDonald, K., Dinardo, S.J., Miller, C.E., Wofsy, S.C., Chang, R.Y.W., 2018. Estimating regional-scale methane flux and budgets using CARVE aircraft measurements over Alaska. Atmos. Chem. Phys. 18, 185–202. https://doi.org/10.5194/acp-18-185-2018

Heimburger, A.M.F., Harvey, R.M., Shepson, P.B., Stirm, B.H., Gore, C., Turnbull, J., Cambaliza, M.O.L., Salmon, O.E., Kerlo, A.-E.M., Lavoie, T.N., Davis, K.J., Lauvaux, T., Karion, A., Sweeney, C., Brewer, W.A., Hardesty, R.M., Gurney, K.R., 2017. Assessing the optimized precision of the aircraft mass balance method for measurement of urban greenhouse gas emission rates through averaging. Elem Sci Anth 5, 26. https://doi.org/10.1525/elementa.134

Hollister, J., 2017. Access Elevation Data from Various APIs.

Hugelius, G., Strauss, J., Zubrzycki, S., Harden, J.W., Schuur, E.A.G., Ping, C.L., Schirrmeister, L., Grosse, G., Michaelson, G.J., Koven, C.D., O'Donnell, J.A., Elberling, B., Mishra, U., Camill, P., Yu, Z., Palmtag, J., Kuhry, P., 2014. Estimated stocks of circumpolar permafrost carbon with quantified uncertainty ranges and identified data gaps. Biogeosciences 11, 6573–6593. https://doi.org/10.5194/bg-11-6573-2014

Karion, A., Sweeney, C., Kort, E.A., Shepson, P.B., Brewer, A., Cambaliza, M., Conley, S.A., Davis, K., Deng, A., Hardesty, M., Herndon, S.C., Lauvaux, T., Lavoie, T., Lyon, D., Newberger, T., Pétron, G., Rella, C., Smith, M., Wolter, S., Yacovitch, T.I., Tans, P., 2015. Aircraft-Based Estimate of Total Methane Emissions from the Barnett Shale Region. Environ. Sci. Technol. 49, 8124–8131. https://doi.org/10.1021/acs.est.5b00217

Karion, A., Sweeney, C., Pétron, G., Frost, G., Michael Hardesty, R., Kofler, J., Miller, B.R., Newberger, T., Wolter, S., Banta, R., Brewer, A., Dlugokencky, E., Lang, P., Montzka, S.A., Schnell, R., Tans, P., Trainer, M., Zamora, R., Conley, S., 2013. Methane emissions estimate from airborne measurements over a western United States natural gas field. Geophys. Res. Lett. 40, 4393–4397. https://doi.org/10.1002/grl.50811

Lin, J.C., Gerbig, C., Wofsy, S.C., Andrews, A.E., Daube, B.C., Davis, K.J., Grainger, C.A., 2003. A near-field tool for simulating the upstream influence of atmospheric observations : The Stochastic Time-Inverted Lagrangian Transport (STILT) model 108. https://doi.org/10.1029/2002JD003161

Marchese, A.J., Vaughn, T.L., Zimmerle, D.J., Martinez, D.M., Williams, L.L., Robinson, A.L., Mitchell, A.L., Subramanian, R., Tkacik, D.S., Roscioli, J.R., Herndon, S.C., 2015. Methane Emissions from United States Natural Gas Gathering and Processing. Environ. Sci. Technol. 49, 10718–10727. https://doi.org/10.1021/acs.est.5b02275

McGuire, A.D., Christensen, T.R., Hayes, D., Heroult, A., Euskirchen, E., Kimball, J.S., Koven, C., Lafleur, P., Miller, P.A., Oechel, W., Peylin, P., Williams, M., Yi, Y., 2012. An assessment of the carbon balance of Arctic tundra: Comparisons among observations,

process models, and atmospheric inversions. Biogeosciences 9, 3185–3204. https://doi.org/10.5194/bg-9-3185-2012

McManus, J., Shorter, J., Nelson, D., Zahniser, M., Glenn, D., McGovern, R., 2008. Quantum Cascade Laser Instrument With Compact Design for Rapid, High Sensivity Measurements of Trace Gases in Air. Appl. Phys. B 92, 387–392.

Miller, S.M., Miller, C.E., Commane, R., Chang, R.Y.W., Dinardo, S.J., Henderson, J.M., Karion, A., Lindaas, J., Melton, J.R., Miller, J.B., Sweeney, C., Wofsy, S.C., Michalak, A.M., 2016. A multiyear estimate of methane fluxes in Alaska from CARVE atmospheric observations. Global Biogeochem. Cycles 30, 1441–1453. https://doi.org/10.1002/2016GB005419

Parazoo, N.C., Commane, R., Wofsy, S.C., Koven, C.D., Sweeney, C., Lawrence, D.M., Lindaas, J., Chang, R.Y.-W., Miller, C.E., 2016. Detecting regional patterns of changing CO_2 flux in Alaska. Proc. Natl. Acad. Sci. 113, 7733–7738. https://doi.org/10.1073/pnas.1601085113

Pearson, G., Davies, F., Collier, C., 2009. An analysis of the performance of the UFAM pulsed Doppler lidar for observing the boundary layer. J. Atmos. Ocean. Technol. 26, 240–250. https://doi.org/10.1175/2008JTECHA1128.1

Peischl, J., Karion, A., Sweeney, C., Kort, E.A., Smith, M.L., Brandt, A.R., Yeskoo, T., Aikin, K.C., Conley, S.A., Gvakharia, A., Trainer, M., Wolter, S., Ryerson, T.B., 2016. Locating and quantifying greenhouse gas emissions at a geological CO 2 storage site using atmospheric modeling and measurements. J. Geophys. Res. Atmos. 119(18), 10,959-10,979. https://doi.org/10.1002/2015JD024631.Received

Pétron, G., Karion, A., Sweeney, C., Miller, B.R., Montzka, S.A., Frost, G.J., Trainer, M., Tans, P., Andrews, A., Kofler, J., Helmig, D., Guenther, D., Dlugokencky, E., Lang, P., Newberger, T., Wolter, S., Hall, B., Novelli, P., Brewer, A., Conley, S., Hardesty, M., Banta, R., White, A., Noone, D., Wolfe, D., Russ Schnell, 2014. A new look at methane and nonmethane hydrocarbon emissions from oil and natural gas operations in the Colorado Denver-Julesburg Basin. J. Geophys. Res. Atmos. https://doi.org/10.1002/2013JD021272

Rella, C.W., Chen, H., Andrews, A.E., Filges, A., Gerbig, C., Hatakka, J., Karion, A., Miles, N.L., Richardson, S.J., Steinbacher, M., Sweeney, C., Wastine, B., Zellweger, C., 2013. High accuracy measurements of dry mole fractions of carbon dioxide and methane in humid air. Atmos. Meas. Tech. 6, 837–860. https://doi.org/10.5194/amt-6-837-2013

Sayres, D.S., Dobosy, R., Healy, C., Dumas, E., Kochendorfer, J., Munster, J., Wilkerson, J., Baker, B., Anderson, J.G., 2017. Arctic regional methane fluxes by ecotope as derived using eddy covariance from a low-flying aircraft. Atmos. Chem. Phys. 17, 8619–8633. https://doi.org/10.5194/acp-17-8619-2017

Stein, A.F., Draxler, R.R., Rolph, G.D., Stunder, B.J.B., Cohen, M.D., Ngan, F., 2015. Noaa's hysplit atmospheric transport and dispersion modeling system. Bull. Am. Meteorol. Soc. 96, 2059–2077. https://doi.org/10.1175/BAMS-D-14-00110.1

Sweeney, C., Dlugokencky, E., Miller, C.E., Wofsy, S., Karion, A., Dinardo, S., Chang, R.Y.-W., Miller, J.B., Bruhwiler, L., Crotwell, A.M., Newberger, T., McKain, K., Stone, R.S., Wolter, S.E., Lang, P.E., Tans, P., 2016. No significant increase in long-term CH<inf>4</inf> emissions on North Slope of Alaska despite significant increase in air temperature. Geophys. Res. Lett. 43, 1–9. https://doi.org/10.1002/2016GL069292

Sweeney, C., Dlugokencky, E., Miller, C.E., Wofsy, S., Karion, A., Dinardo, S., Chang, R.Y., Miller, J.B., Bruhwiler, L., Crotwell, A.M., Newberger, T., Mckain, K., Stone, R.S., Wolter,

S.E., Lang, P.E., Tans, P., 2016. No significant increase in long-term CH4 emissions on North Slope of Alaska despite significant increase in air temperature. Geophys. Res. Lett. doi:10.1002/2016GL069292. https://doi.org/10.1002/2016GL069292.Received

Sweeney, C., Karion, A., Wolter, S., Newberger, T., Guenther, D., Higgs, J.A., Andrews, A.E., Lang, P.M., Neff, D., Dlugokencky, E., Miller, J.B., Montzka, S.A., Miller, B.R., Masarie, K.A., Biraud, S.C., Novelli, P.C., Crotwell, M., Crotwell, A.M., Thoning, K., Tans, P.P., 2015. Seasonal climatology of CO2 across north america from aircraft measurements in the NOAA/ESRL global greenhouse gas reference network. J. Geophys. Res. 120, 5155–5190. https://doi.org/10.1002/2014JD022591

Yacovitch, T.I., Herndon, S.C., Roscioli, J.R., Floerchinger, C., McGovern, R.M., Agnese, M., Pétron, G., Kofler, J., Sweeney, C., Karion, A., Conley, S.A., Kort, E.A., Nähle, L., Fischer, M., Hildebrandt, L., Koeth, J., McManus, J.B., Nelson, D.D., Zahniser, M.S., Kolb, C.E., 2014. Demonstration of an ethane spectrometer for methane source identification. Environ. Sci. Technol. 48, 8028–8034. https://doi.org/10.1021/es501475q

Zona, D., Gioli, B., Commane, R., Lindaas, J., Wofsy, S.C., Miller, C.E., Dinardo, S.J., Dengel, S., Sweeney, C., Karion, A., Chang, R.Y.-W., Henderson, J.M., Murphy, P.C., Goodrich, J.P., Moreaux, V., Liljedahl, A., Watts, J.D., Kimball, J.S., Lipson, D.A., Oechel, W.C., 2016. Cold season emissions dominate the Arctic tundra methane budget. Proc. Natl. Acad. Sci. 113, 40–45. https://doi.org/10.1073/pnas.1516017113